Electric–Magnetic–Electric Slow-Wave Microstrip Line and Bandpass Filter of Compressed Size

Ching-Kuo Wu, *Student Member, IEEE*, Hsien-Shun Wu, *Member, IEEE*, and Ching-Kuang Cliver Tzuang, *Fellow, IEEE*

***Abstract*—This paper presents a novel integrated microstrip low-loss slow-wave line. The new microstrip replaces the conventional metal strip by composite metals paralleling the electric surface and magnetic surface (MS). The MS made of an array of coupled inductors shows a high-impedance state in the stopband, below which the propagation properties can be well controlled by varying the dimensions of the electric surface and MS. The dispersion curves obtained by matrix-pencil analyses closely correspond to those obtained by scattering-parameter extraction. Theoretical results, as confirmed experimentally, indicate that an increase of over 60% in the slow-wave factor can be achieved without sacrificing propagation losses, using the proposed structure. This electric–magnetic–electric (EME) microstrip is insensitive to the alignment position of the periodical structure, and can be constructed using conventional printed-circuit-board fabrication processes and integrated with other microwave components in a multilayered circuit. A compact EME bandpass filter (BPF) with suppressed harmonic responses is presented. The length of the filter is reduced by 26%, and the measured insertion loss and fractional bandwidth is comparable to that of a conventional microstrip BPF on the same substrate.**

***Index Terms*—Bandpass filters, matrix-pencil method, microstrip, slow-wave structures.**

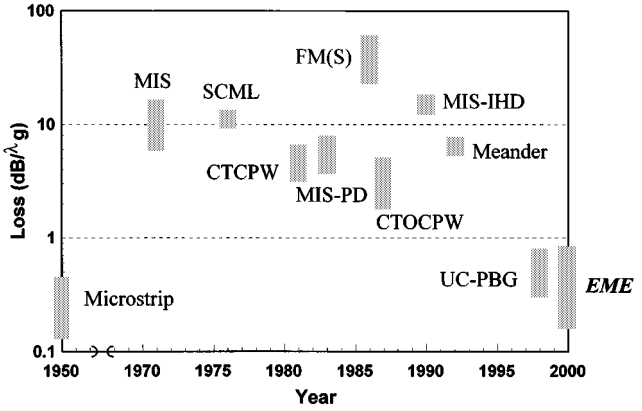

Fig. 1. Losses of slow-wave lines. The operating frequency is below 6 GHz. MIS = metal–insulator–semiconductor microstrip line. SCML = Schottky-contact microstrip line. FM(S) = ferromagnetic (semiconductor) microstrip line. MIS-IHD = inhomogeneously doped MIS transmission line. MIS-PD = periodically doped MIS transmission line. CTCPW = cross-tie coplanar waveguide. CTOCPW = cross-tie overlay coplanar waveguide. UC-PBG = microstrip line with uniplanar compact photonic bandgap ground plane. EME = electro–magnetic–electric microstrip line.

I. Introduction

REDUCTION of circuit dimensions in both hybrid and monolithic microwave integrated circuits (MMICs) is important from the cost and reliability point-of-view. Passive devices, especially those designed with distributed transmission lines, occupy most space. Slow-wave propagation by separating electric and magnetic energies has been investigated as a method to reduce the transmission-line length for a given insertion phase. Fig. 1 lists a few representative works of slow-wave transmission lines from the past 30 years. The unit for the vertical axis is dB/λg, where λg is the guided wavelength. This is a reasonable choice of unit for a fair comparison of losses associated with various slow-wave lines since all known methods for enhancing the slow-wave factor (SWF), also known as the normalized phase constant, lead to an increasing attenuation constant.

Slow-wave transmission lines such as the metal–insulator–semiconductor (MIS) microstrip, ferromagnetic (FM) microstrip, ferromagnetic semiconductor (FMS) microstrip, or Schottky-contact microstrip line (SCML) configurations using (FM) semiconductor surface layers were extensively investigated several years ago [1]–[5]. These slow-wave lines, which incorporate layered substrates, show losses near 10 dB/λg. Moreover, increasing the operating frequency degrades the SWF [5]–[7]. However, these uniform guiding structures have greatly improved the SWF. Within the low-frequency range, high-Q factors can be obtained with nearly optimum conditions [8].

Some modified structures use inhomogeneous doping (MIS-IHD) [9] or periodically doped substrates (MIS-PD) [10] for the MIS or Schottky coplanar waveguide to reduce the attenuation and enhance the SWF, thus extending the slow-wave propagation frequency range. Several periodic structures such as the cross-tie coplanar waveguide (CTCPW) [11], cross-tie-overlay coplanar waveguide (CTOCPW) [12], and meander microstrip [13] have been proposed to improve the performance of slow-wave transmission lines. These improved slow-wave lines have losses between 1–10 dB/λg. Notice that improved slow-wave lines employ complicated fabrication process and still have higher insertion losses than that of a conventional microstrip line [14].

Microstrips that incorporate a photonic bandgap (PBG) structure and experience periodic perturbations from the substrate [15], ground plane [14], [16], or transmission line itself [17] have recently shown great potential for a great variety of applications in microwave electronics and antenna development [18],

Manuscript received October 23, 2001. This work was supported by the Ministry of Education of Taiwan under Grant 89-E-FA06-2-4, and by the National Science Council under Grant NSC 91-2213-E-009-045.

The authors are with the Institute of Electrical Communication Engineering, National Chiao Tung University, Hsinchu, Taiwan 300, R.O.C. (e-mail: cktzuang@cc.nctu.edu.tw).

Publisher Item Identifier 10.1109/TMTT.2002.801355.

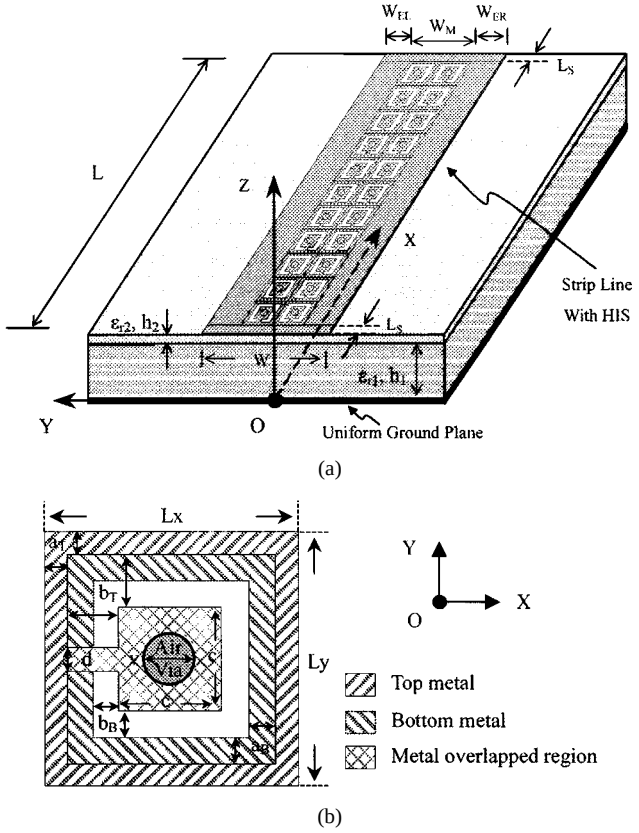

Fig. 2. (a) Three-dimensional view of the proposed microstrip line with a metal strip replaced by EME surfaces. (b) Top view of the 2-D HIS unit cell on the top/bottom of a thin substrate (ε_{r2}, h_2).

[19]. One of the most interesting applications of such PBG structures exhibits a significant increase in the SWF without much loss for a microstrip on a uniplanar compact photonic bandgap (UC-PBG) ground plane. As shown in Fig. 1, the microstrip on the UC-PBG ground plane further reduces the loss, representing the first breakthrough of the 1-dB/λg barrier after decades of effort to improve slow-wave lines.

In practice, a conductor-backing ground plane for integrating microwave modules is often desired. Therefore, this paper presents a novel microstrip slow-wave structure that incorporates a uniform ground plane and uses PBG structures alongside the signal line in the axial direction, as depicted in Fig. 2. Like the UC-PBG, the new PBG cells exhibit a high-impedance surface (HIS) state in a certain frequency band and behave like a magnetic surface (MS) by reflecting the incoming electromagnetic wave without reversing its phase. The signal line consists of both a magnetic and an electric surface. When viewed from the transverse plane of the proposed slow-wave microstrip structure, the electric and MSs are arranged in electric–magnetic–electric (EME) order; thus, the microstrip is named the "EME composite." The propagation losses of the proposed EME microstrip match those of a conventional microstrip (see Fig. 1). Additionally, the EME microstrip is insensitive to the alignment position of the PBG structure. The EME microstrip structure can also integrate other conventional microstrip components, and does not interact with components on the other side of the continuous ground plane in a multilayered circuit.

The remainder of this paper is organized as follows. Section II describes the theory and design of the EME microstrip. Section III reports the corresponding scattering analyses, which are compared and validated by measurements. The extracted values of the propagation constants and characteristic impedances, derived from the scattering analyses of various microstrip structures, are presented to demonstrate the generality of the EME microstrip configuration. Two theoretical methods are employed to confirm the validity of the reported transmission-line data. The losses of the proposed EME microstrip are also discussed. Section IV considers the influence of varying the MS position and filling percentage in the composite EME metal strip on the propagation property of the EME microstrip. Section V presents a bandpass filter (BPF) application example. The attractive features of the EME microstrip BPF structure are observed, theoretically and experimentally, to be low loss, reduced size, and suppression of harmonic resonance. Conclusions are then made in Section VI.

II. Principles and Operation of the EME Microstrip

The novel EME line is like a conventional microstrip on a continuous uniform ground plane, except that the metal strip is a sheet of composite metal made of EME surfaces (Fig. 2). The electrical surface is a plain ordinary metal strip of a certain thickness. Coupled connected metallic coils realize the MS. Each metallic coil is viewed as a unit cell. Thus, the coils form a periodic array in the central plane of the microstrip. The entire array resonates at a certain bandwidth, namely, the stopband, and the connected metallic surface enters a high-impedance state [20], [21]. The guiding structure proposed for typical applications is symmetrical about its central plane, which is a magnetic (electric) wall for the microstrip even (odd)-mode operation. Note that the MS is frequency dependent, implying that the impedance of the MS is sufficiently high at a certain frequency band. In view of the frequency-dependent MS at the central plane, the odd-mode dispersion characteristics change accordingly. This paper, however, focuses on even-mode propagation and effectively offers beneficial applications when an increased SWF, higher characteristic impedance, and high-Q factor are desired for a microstrip.

The new PBG structure used in this proposed EME microstrip is made on both sides of a thin substrate. Each side of the unit cell has one coupled spiral inductors (coils), as depicted in Fig. 2(b). The coupled coils are connected by the center metal via through the thin substrate. Narrowing the arm widths (a_T, a_B) enlarge the inductance, but reduce the capacitance that come from the fringing electric fields between or within the two adjacent coils. Note that the stopband frequency is much higher than the operating frequency of the EME microstrip, as discussed in Section III. In the design presented here, the first stopband of the PBG structure is at 10 GHz with cells of size 2.134 mm (Lx) $\times$ 2.134 mm (Ly) (7.1% of free-space wavelength at 10 GHz). The presence of the MS alters the modal current distributions along the transverse and longitudinal directions of the guide, thereby changing the dispersion characteristics of the microstrip.

Although the cell size has been maintained relatively low compared to the free-space wavelength (λo), such microstrip

cannot be used in many applications when propagation properties must be finely adjusted. Adding electric surfaces alongside the MS, forming EME surfaces, allows an additional degree of freedom for varying the propagation characteristics. Proper widths (W_{EL}, W_{ER}, and W_M) of the electric and MSs, respectively, can be chosen to obtain the required propagation constant, characteristic impedance, and stopband bandwidth of the transmission line.

The EME microstrip is compatible with modern state-of-the-art multilayer printed circuit technology. Referring to Fig. 2(a), the electric and MSs are made on a two-sided printed RO4003 circuit board of thickness (h_2) 0.203 mm and relative permittivity (ε_{r2}) of 3.38; the EME composite strip is then glued to a conductor-backing RO4003 substrate of thickness (h_1) 0.508 mm under proper heat and pressure to complete the EME microstrip as a slow-wave line.

III. Propagation Characteristics of EME Microstrip and Validity Checks

A. Scattering Analyses

Two 4.268-mm-wide (W) EME microstrip prototypes are built and tested (see Fig. 2). Each EME microstrip is 32.01-mm long (L), corresponding to 15 unit cells. A short 1-mm-long (L_S) metal strip is added at each end of the EME microstrip to facilitate the pin contact to the WILTRON 3680-K test fixture. The effect of these two short pieces of microstrips has been included in the numerical simulations. The first EME microstrip has $W_{EL} = W_{ER} = 1.067$ mm and $W_M = 2.134$ mm, with one cell in the transverse direction; the EME microstrip is said to have a 50% filling of the MS. The second EME microstrip has $W_M = 4.268$ mm, with two cells in the transverse direction and no electric surface at all. In such a case, the microstrip is an MS microstrip, corresponding to 100% filling of the MS.

The coils on the top layer of the 0.203-mm-thick (h_2) substrate have the following dimensions. The outer coil is 0.127-mm wide (a_T) in both the x- and y-directions, the inner square coil is 0.864-mm wide (c), and a metal patch of 0.254 mm (d) $\times$ 0.508 mm (b_T) connects the outer and inner coils. On the bottom of the substrate, the outer coil is 0.254-mm wide (a_B), the inner square coil is 0.864-mm wide (c), and the connecting metal patch is 0.254 mm (d) $\times$ 0.254 mm (b_B). The top and bottom coils are connected by a vertical conducting via with a diameter of 0.406 mm (v). The unit cells are connected to adjacent cells on the top layer. The unit cell with a much small area can be fabricated by commercial semiconductor technologies. The above arrangement allows fast evaluation of the proposed concept. The electric and MSs are also built using the conventional printed-circuit-board processing technology, including the via through-hole plating.

The scattering parameters of these two EME microstrips are measured and compared with those obtained by a full-wave solver (Zeland IE3D) using the integral-equation method. Throughout the numeric analyses, the conductivity and thickness of the metal is assumed to be 4.9×10^7 S/m and 0.018 mm, and the loss tangent of the substrate is assumed to be 2×10^{-3}. Fig. 3 plots the theoretic and measured results for S_{11} and S_{21}, showing excellent agreement in all cases. The measured scattering parameters are consistently shifted to the right-hand side by approximately 0.3 GHz. Careful examination of the prototype indicates a slightly excessive etching (approximately 12 μm), resulting in a decrease in the coupling between adjacent cells and thereby shifting the scattering parameters. Fig. 3(a) and (b) shows that the stopband for the 50% filling case is between 8.5 GHz (f_1) and 10.5 GHz (f_2) and centered at 9.5 GHz (f_0). The 100% filling case has a wider stopband, i.e., between 8.0 GHz (f_1) and 11.75 GHz (f_2), with the center frequency at 9.875 GHz (f_0), as shown in Fig. 3(c) and (d). The fractional bandwidth ($(f_2 - f_1)/f_0$) increases from 21% to 38% when the MS filling percentage increases from 50% to 100%. Inside the stopband, the reflection coefficient is nearly unity (0.95) and the transmission coefficient is lower than -20 dB. In the lower frequency region that interests us, the EME microstrip shows very good transmission characteristics with low reflection, although it is not exactly matched to the measurement system of 50-Ω impedance. Additionally, the EME microstrip is a good guiding structure with little distortion due to the linear phase variation of S_{21} with frequency. A faster phase variation of S_{21} exhibits more improved slow-wave phenomena as the PBG filling percentage is increased.

B. Dispersion Characteristics

The periodic modulation of the MS on the familiar microstrip mode launched at either end of the EME microstrip yields space harmonics on the excited currents [22], [23]. These harmonics can be extracted by the matrix-pencil method [24]. Fig. 4 shows the vectored current distributions, obtained by full-wave simulations of the EME microstrip with a 50% PBG filling percentage for the uniform ground plane. At 5 GHz (outside the stopband), a large current flows beneath the composite EME strip, i.e., between $y = -2.134$ and $y = 2.134$ mm, from the input terminal ($x = 0$) to the output terminal ($x = 34.01$ mm), without a noticeable decay. The current distributions resemble the dominant mode of a typical microstrip, except the shorter distance of adjacent phase reversal positions than the uniform microstrip.

The extraction of space harmonics on the excited currents manifests the similarity between the Fourier series expansion of a periodic function and the space–harmonics representation of a PBG structure [23]. The space harmonic is denoted by its complex propagation constant $\gamma^{\pm}_{m,n}$, $(\beta^{\pm}_{m,n} - j\alpha^{\pm}_{m,n})$, which represents a traveling-wave component of the nth higher order space component associated with the EH_m mode: superscript $+$ $(-)$ signifies the forward (backward) traveling wave. Matrix-pencil analyses show that a forward traveling wave, denoted by its complex propagation constant $\gamma^{+}_{0,0}$, and a backward traveling wave, denoted by $\gamma^{-}_{0,0}$, are the only two major space harmonics for an operating frequency below 8 GHz. Both $\gamma^{+}_{0,0}$ and $\gamma^{-}_{0,0}$ have the same phase constant, but with opposite signs. As shown in Fig. 5, the matrix-pencil signal analyses of the ground returned currents along various Y cuts of Fig. 4, indicate that extracted values are insensitive to the chosen current cut for the entire spectrum of interest.

Fig. 6 displays the normalized phase constant of the forward traveling-wave component for the EME microstrip with

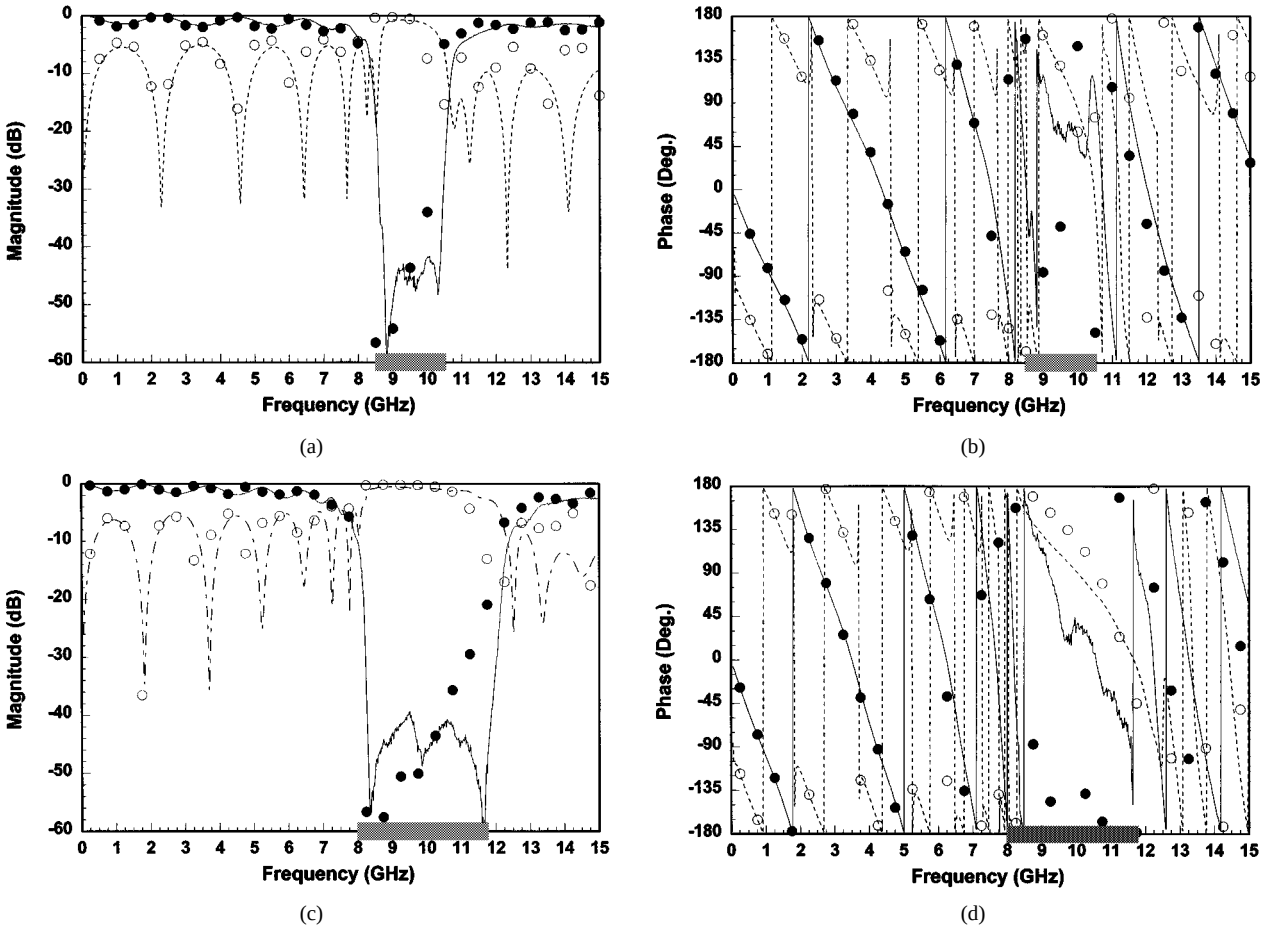

Fig. 3. Magnitude and phase of scattering parameters for the EME microstrip with: (a), (b) 50% and (c), (d) 100% PBG filling percentages. ◯: simulated S_{11}. - - - - - : measured S_{11}. •: simulated S_{21}. ——: measured S_{21}. Gray bar: stopband region.

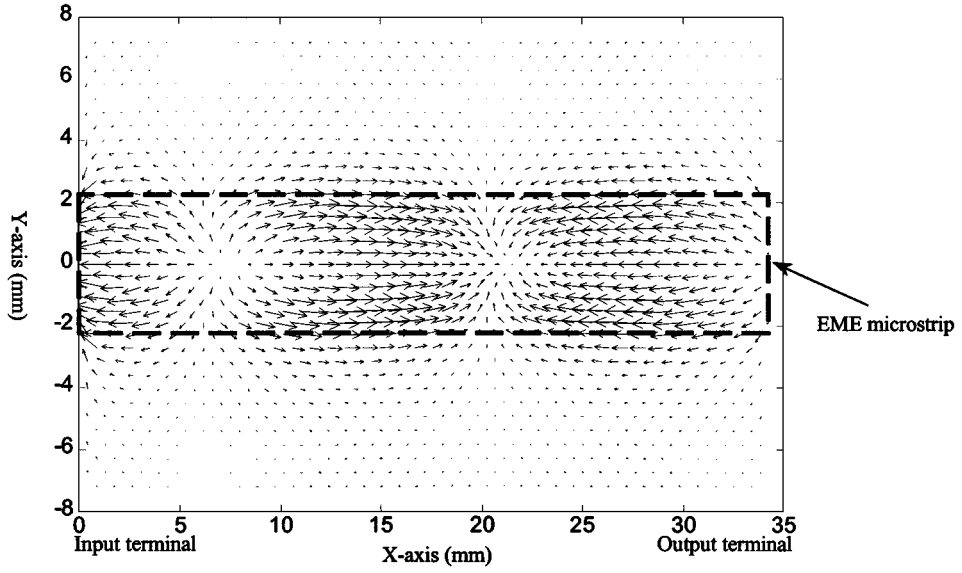

Fig. 4. Vectored current distributions in the uniform ground plane beneath the EME microstrip with 50% PBG filling percentage at 5 GHz.

different PBG filling percentages. A sharp rise is observed at 8.5 GHz for the 50% filling case, and at 8.0 GHz for the 100% filling case. The peak frequencies of the normalized phase constant are near the lower corner frequencies of the stopband in both cases.

In the lower frequency region, the $\gamma_{0,0}^{+}$ wave dominates and the unit cell size of the PBG structure is less than 0.06 λo (at 8 GHz). The complex propagation constant and characteristic impedance (Zc) can be estimated from the simulated andmeasured scattering parameters (Sij) referenced to the Zo im-

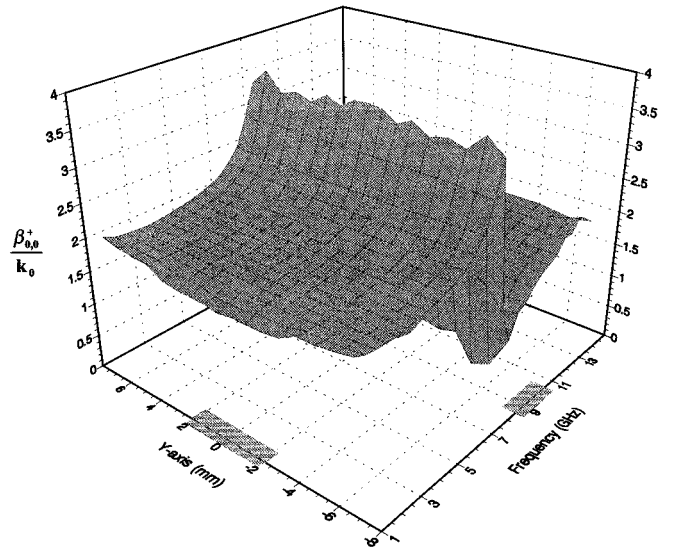

Fig. 5. SWF distributions extracted by matrix-pencil analyses from ground returned currents along various Y cuts for the EME microstrip with 50% PBG filling percentage.

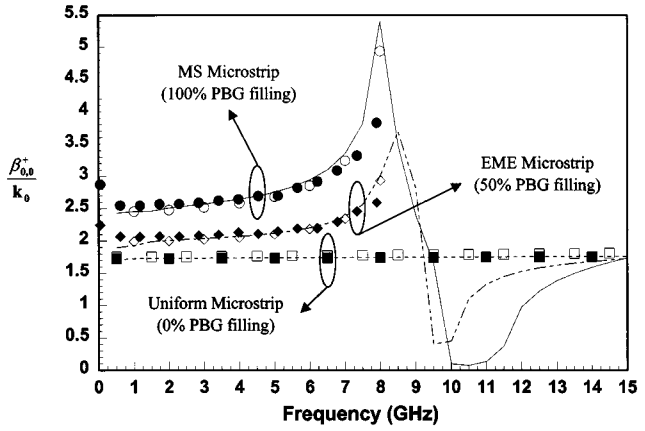

Fig. 6. Comparison of SWFs for the MS microstrip, EME microstrip, and uniform microstrip. Case 1: MS microstrip. ——: matrix-pencil analysis. ◯: simu. [S] extraction. •: meas. [S] extraction. Case 2: EME microstrip. —·—: matrix-pencil analysis. ◇: simu. [S] extraction. ◆: meas. [S] extraction. Case 3: Uniform microstrip. - - - - -: matrix-pencil analysis. □: simu. [S] extraction. ■: Agilent EEsof LineCalc.

pedance level by the following equations [25]:

$$e^{j\gamma^+_{0,0}L} = \frac{1-S_{11}^2+S_{21}^2+\sqrt{(1+S_{11}^2-S_{21}^2)^2-(2S_{11})^2}}{2S_{21}} \quad (1)$$

$$Z_C = Z_0\sqrt{\frac{(1+S_{11})^2-S_{21}^2}{(1-S_{11})^2-S_{21}^2}}. \quad (2)$$

The dispersion curve of a conventional microstrip (0% MS filling) with the same width ($W_{EL} = 4.268$ mm, $W_M = W_{ER} = 0$), and length ($L = 32.01$ mm) is also calculated through its predicted scattering parameters. These results are superimposed for comparison and the dispersion curves obtained by the matrix-pencil analyses, S-parameter extraction and Agilent EEsof LineCalc are shown to agree closely.

Fig. 6 reveals that the SWF of the EME microstrip is flat until the operating frequency approaches the lower corner of the stopband frequency. The uniform microstrip shows an SWF of 1.736 at 5 GHz, whereas the 50% MS EME microstrip increases the SWF by 22% to 2.12 and the 100% MS microstrip increases the SWF by 60% to 2.757. Such increases in the SWF by 22%–60% suggest that the proposed EME microstrip is a viable approach for designing a slow-wave line. Further optimization of the EME microstrip is thought to be able to increase the SWF.

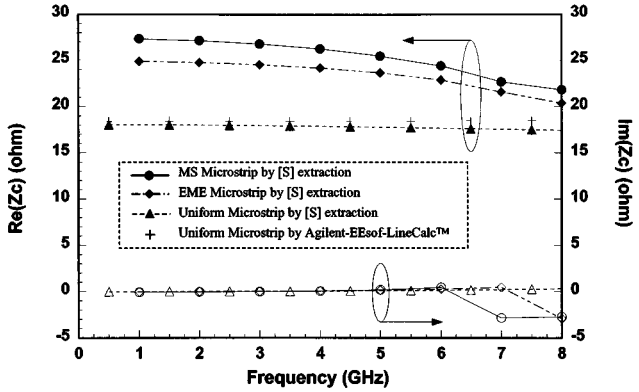

Fig. 7. Comparison of the real part (solid symbol) and imaginary part (hollow symbol) of characteristic impedances (Zc) for the EME microstrip with different PBG filling percentages.

The line length of EME microstrip has relatively small influences on the converged values of extracted characteristic impedance, except at frequencies where the line length is near a multiple of half-wavelength. Based on the convergence study, we choose 6.402-mm-long (L) EME microstrip, corresponding to three unit cells in the longitudinal direction, to obtain the estimated characteristic impedance. Fig. 7 displays the real and imaginary parts of the characteristic impedance of these EME microstrip lines, with those of a uniform microstrip on the same 0.508-mm-thick substrate with a relative permittivity of 3.38. Below the stopband frequencies, the characteristic impedances are almost purely real. Approaching the stopband frequencies from the lower frequency region, complex characteristic impedances emerge, representing the losses to be investigated later in this paper. In the particular case studies, the characteristic impedance of the EME microstrip increases by 33% for 50% filling and by 43% for 100% filling at 5 GHz. These results imply that the PBG structure that partially occupies the metal strip increases the distributed inductance per unit length, thereby simultaneously increasing SWF and Z_C [25]. The characteristic impedance slightly decreases as the frequency increases toward the stopband. Nevertheless, in contrast to most slow-wave structures, the problems of low SWF and low characteristic impedance at high frequency do not exist when the operating frequencies are below the stopband.

C. Losses

The increase in SWF alone does not establish the usefulness of the EME microstrip as a slow-wave line. The EME microstrip must also possess low-loss characteristics. The loss of the EME microstrip is divided into two parts, i.e., the low-frequency region suitable for slow-wave propagation and the high-frequency region near and above the lower corner frequency of

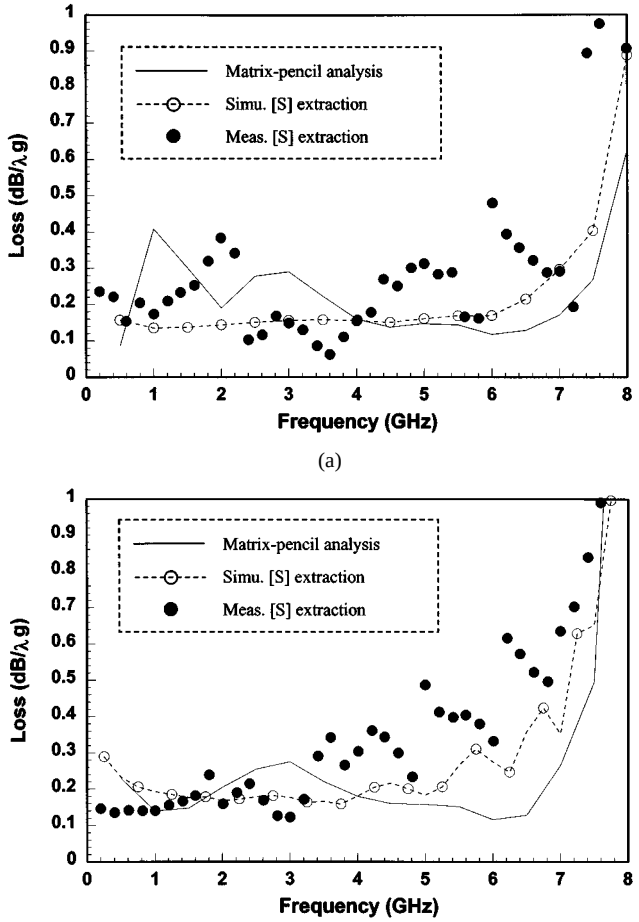

Fig. 8. Loss per guided wavelength obtained by matrix-pencil analysis and scattering parameter extraction for the EME microstrip with: (a) 50% and (b) 100% PBG filling percentages.

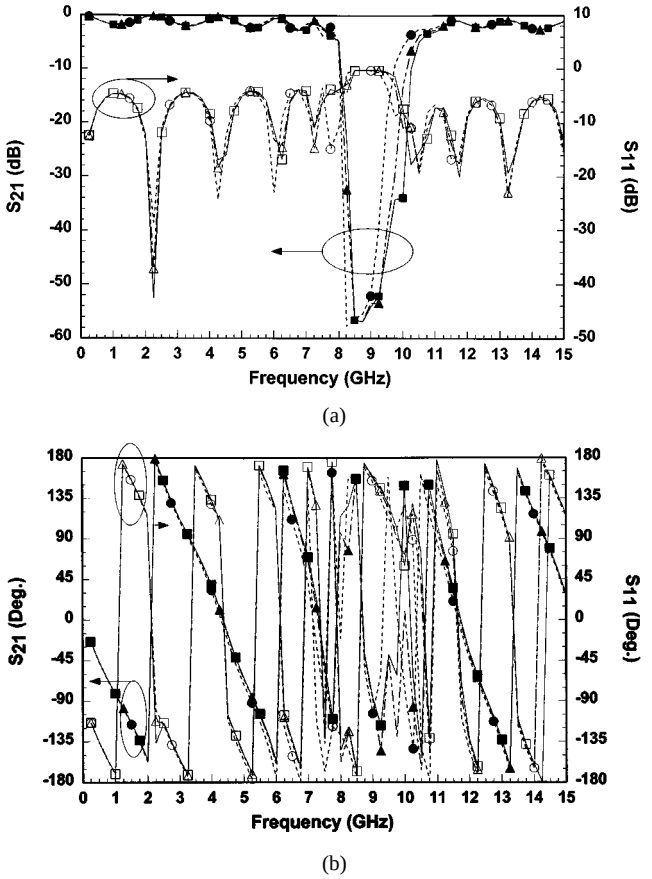

Fig. 9. Scattering parameters (solid symbol for S_{21} and hollow symbol for S_{11}) for the EME microstrip with different alignment positions of PBG in the transverse plane. (a) Magnitude. (b) Phase. - - -●- - -: $W_{EL} = 0$ mm, $W_M = 2.134$ mm, $W_{ER} = 2.134$ mm. —···▲···—: $W_{EL} = 0.534$ mm, $W_M = 2.134$ mm, $W_{ER} = 1.6$ mm. —■—: $W_{EL} = 1.067$ mm, $W_M = 2.134$ mm, $W_{ER} = 1.067$ mm.

the stopband. Matrix-pencil analyses of the EME microstrips, as reported in Fig. 6, show that more than one space harmonic prevail at frequencies near and above the stopband. Some of the space harmonics enter the radiation region of the Brillouin diagram. Fig. 8 plots the attenuation constant, in decibels per unit guided wavelength of the forward traveling-wave component obtained by matrix-pencil analyses for various EME microstrips with different PBG filling percentages. The results agree well with the corresponding values obtained by analyzing the scattering parameters, as reported in Fig. 3. Large measured losses (exceeding 1.0 dB/λg) occurred near the corner frequency of the stopband, i.e., 8.5 GHz for the EME microstrip (50% filling), and 8.0 GHz for the MS microstrip (100% filling). Thus, operation near the lower corner frequency of the stopband should be avoided when applying the EME microstrip as a low-loss slow-wave line. The operating frequencies of the EME microstrip should be restricted. In this particular case study, the upper bound frequency is near 5 GHz.

The measured loss per guided wavelength of the EME microstrip is 0.3 dB/λg for 50% filling and 0.48 dB/λg for 100% filling at 5 GHz. These values slightly exceed that of the corresponding uniform microstrip (0.2 dB/λg). In any case, EME microstrips show a slight increase in loss. Therefore, the SWF may be increased with only a token increase in loss.

IV. EME Microstrip Design Chart

A. Influence of Symmetry on EME Microstrip

The sensitivity of stopband behavior to the alignment offset of the PBG structure in the EME microstrip must be considered. Fig. 9 shows the predicted scattering parameters. The impact of unbalanced symmetry caused by variations in electric surface dimensions may create problems as the even-mode operation of the EME microstrip is preferred. Maintaining the same overall width of the EME surfaces ($W = 4.268$ mm), the following three cases are simulated using the 1×15 PBG array as the MS, where $W_M = 2.134$ mm and $L = 32.01$ mm.

Case 1) The PBG is placed at the left-most edge, i.e., $W_{EL} = 0$, $W_{ER} = 2.134$ mm.

Case 2) Electric surface dimensions are unequal, i.e., $W_{EL} = 0.534$ mm, $W_{ER} = 1.6$ mm.

Case 3) PBG is placed in the middle of the composite strip, i.e., $W_{EL} = W_{ER} = 1.067$ mm.

The simulated scattering parameters of these symmetric and asymmetric case studies are almost identical, implying that the dispersion characteristics of the EME microstrip are nearly the same despite the relative position of the PBG structure in the transverse plane, provided the total width of the EME

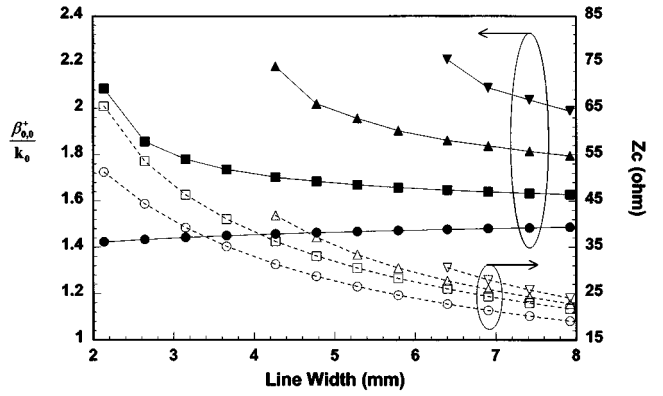

Fig. 10. SWF (solid symbol) and characteristic impedance (hollow symbol) of the EME microstrip with various linewidths (W) and PBG filling percentages at 4.5 GHz. —●—: without MS cell ($M = 0$), i.e., uniform microstrip. —■—: one row of cells ($M = 1$). —▲—: two rows of cells ($M = 2$). —▼—: three rows of cells ($M = 3$).

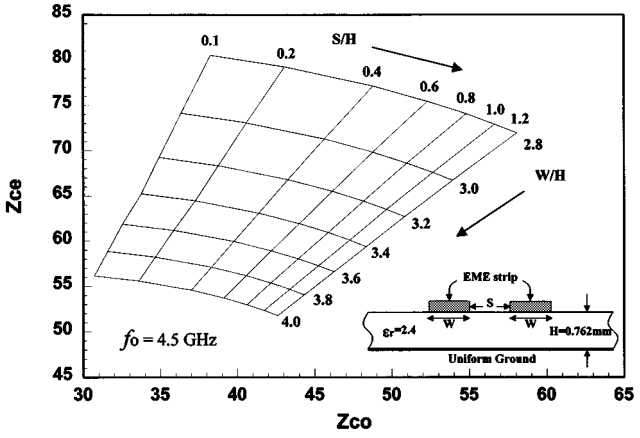

Fig. 11. Even- and odd-mode characteristic-impedance design data for coupled EME microstrips.

microstrip is unchanged. It is favorable for practical applications that the symmetry of the EME microstrip does not significantly alter the propagation characteristics. Note also that the lower stopband corners nearly coincide at around 8 GHz for all three cases where the transmission coefficients fall sharply to below −50 dB. However, the upper edges of the transmission coefficients occur at 9.75, 10, and 10.25 GHz. The symmetrical case ($W_{EL} = W_{ER} = 1.067$ mm) has a wider stopband region than other asymmetric EME microstrip cases; therefore, the symmetric EME microstrip is preferred for filter and antenna applications when the transmission response at harmonic frequencies or surface waves must be suppressed.

B. Design Curves for EME Microstrip

The equivalent inductance and capacitance per unit length of the EME microstrip can be changed by adjusting the percentage of the metal strip and MS, thereby altering the SWF and characteristic impedance. The proposed EME microstrip also imposes its own limitations. The cell, which forms the PBG array and the MS, has finite width. Thus, the EME microstrip cannot be designed with an arbitrarily high impedance level, due to the quantized finite cell size. Designing a smaller PBG cell or using a substrate with a smaller permittivity (ε_1) can remedy such a problem. A family of dispersion curves must be established for the EME microstrips on a substrate with a thickness of 0.762 mm (h_1) and a relative permittivity of 2.4 (ε_{r1}) to facilitate practical implementation of the EME filter shown in Section V. An $M \times N$ PBG array is employed, where N is 3 and M varies from 1 to 3. Steadily increasing the width of the EME microstrip (W) enables more cells (M) in the transverse plane to be adopted. Initially, no cell is included, i.e., $M = 0$, and the EME microstrip is a normal microstrip, yielding the lines with solid (hollow) circle symbols in Fig. 10, which show the normalized phase constant and characteristic impedance of the EME microstrip at 4.5 GHz. Next, one cell in the transverse plane ($M = 1$) is considered and the width of the EME microstrip is further increased by filling the electric surface symmetrically on both sides of the EME microstrip. The results are given by lines with solid (hollow) square symbols. Fig. 10 shows a set of dispersion curves for the same process repeated for $M = 2$ and 3. Given a fixed linewidth (W), the SWF and characteristic impedance increase simultaneously with increasing cell number (M) in the transverse direction for this particular case. Figs. 6 and 7 suggest that further increasing the PBG filling percentage should increase SWF and Zc. Fig. 10 also confirms this conjecture. A higher value of M corresponds to an increased PBG filling percentage, leading to greater perturbation of the current and simultaneous increases in the inductance per unit length; the SWF and characteristic impedance increase accordingly. The design curves in Fig. 10 will be applied to design a BPF centered at 4.5 GHz in the following section.

V. Compressed-Size BPF

Reducing the length of a microwave filter is an immediate application of the low-loss EME microstrip. Unwanted harmonic resonance can also be suppressed by the EME composite structure [19]. A three-resonator 0.5-dB ripple Chebyshev BPF centered at 4.5 GHz with 10% fractional bandwidth is designed and fabricated on an ULTRALAM circuit board with a thickness 0.762 mm and a relative permittivity of 2.4. The design parameters and procedures for an edge-coupled BPF can be found in the literature [26], [27]. Fig. 11 plots the characteristic impedances of the symmetrical EME coupled lines with one cell in the transverse direction for various strip widths (W) and gap spacings (S) at 4.5 GHz. This design graph is employed to determine the necessary strip width (W) and gap spacing (S) for a given set of characteristic impedances Zce (even mode) and Zco (odd mode). Accordingly, the required dimensions of EME coupled lines are 2.387 mm ($W/H = 3.1$) and 0.152 mm ($S/H = 0.2$) for the first and end sections, and 2.793 mm ($W/H = 3.7$) and 0.762 mm ($S/H = 1$) for the two center sections. The quarter-wavelength of the couple line section can be determined from the design curve with one cell in the transverse direction, as shown ($M = 1$) in Fig. 10. The required coupled-line lengths are 8.163 mm for the 2.387-mm-wide sections and 8.635 mm for the 2.793-mm-wide sections, respectively. The small uniform microstrip feed line is 2.54-mm wide and 1.0-mm long, corresponding to a 50-Ω microstrip on the combined substrates. Fig. 12 shows a photograph of the prototype of the EME microstrip edge-coupled BPF and the physical length is 26% less

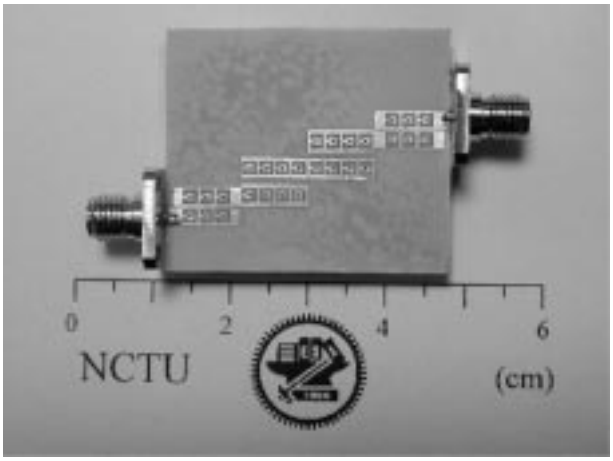

Fig. 12. Photograph of the EME edge-coupled microstrip BPF.

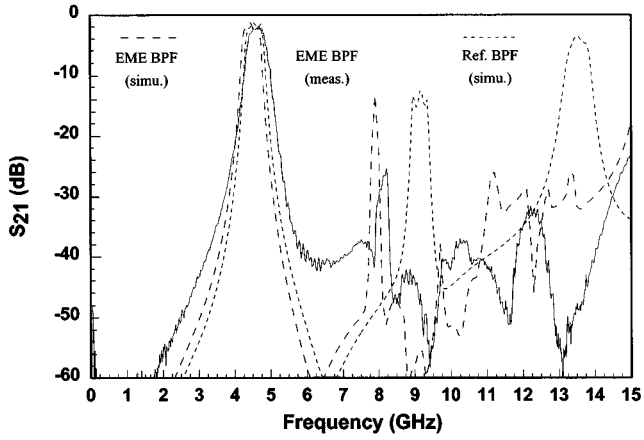

(a)

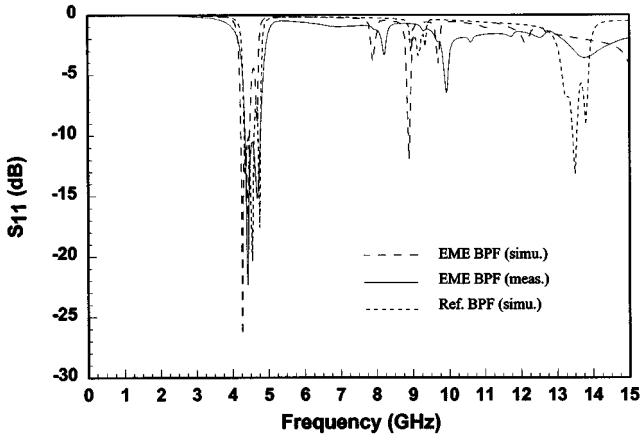

(b)

Fig. 13. Predicted and measured frequency response for the EME coupled microstrip BPF in comparison with that of a conventional BPF. (a) Insertion loss. (b) Return loss.

than that of a conventional microstrip BPF on the same substrate.

Fig. 13(a) and (b) shows the insertion and return losses of the EME microstrip edge-coupled BPF, respectively. The simulated results of a conventional BPF using normal microstrips are also given. The measured passband characteristics exhibit a 11.3% fractional bandwidth and a center frequency of 4.6 GHz, with a minimum insertion loss of 2.0 dB, including the effect of two SMA connectors. The passband loss is slightly higher than the predicted values of the EME BPF and conventional BPF, which are 1.3 and 1.4 dB at 4.5 GHz, respectively. Fig. 13 also shows that the attenuation rate outside the passband is compatible with the conventional BPF. The measured stopband transmission characteristics are approximately 15 dB higher than the predicted values, i.e., between 6–7.5 GHz, and show a significant reduction at the second and third harmonic frequencies. The measured result shows a 40–50-dB suppression, as compared to the values of -13 and -4 dB in the normal microstrip case at 9.0 and 13.5 GHz, respectively. The slight transmission peak (lower than -25 dB) observed near 8 GHz is related to the increased loss values outside and near the stopband frequencies (see Fig. 8).

VI. Conclusion

A novel PBG microstrip line called the EME microstrip has been proposed, analyzed, and tested by experiments. The EME microstrip consists of composite metals paralleling the electric surface and MS, where the MS is made of an array of coupled inductors. This new type of microstrip is easy to fabricate and insensitive to the alignment offset of the PBG structure in the composite metal strip. The results show that EME microstrips exhibit relatively low loss, reasonably large SWFs, convenient values of characteristic impedance, and very little dispersion over a broad range of microwave frequencies.

The low-loss EME microstrip has been employed to design an edge-coupled three-resonator BPF centered at 4.5 GHz with 10% fractional bandwidth. The measured results of this compressed-size BPF show a 2.0-dB minimum insertion loss in the passband and over 40-dB suppression of the spurious responses. This novel EME composite structure should have a wide range of applications for compact and high-performance circuit components in microwave and millimeter-wave integrated circuits.

Acknowledgment

The authors extend special thanks to Prof. T. K. Sarkar, Syracuse University, Syracuse, NY, for kindly supervising the matrix-pencil analyses.

References

[1] H. Hasegawa, M. Furukawa, and H. Yanai, "Properties of microstrip line on Si–SiO_2 system," *IEEE Trans. Microwave Theory Tech.*, vol. MTT-19, pp. 869–881, Nov. 1971.

[2] G. W. Hughes and R. M. White, "Microwave properties of nonlinear MIS and Schottky-barrier microstrip," *IEEE Trans. Electron Devices*, vol. ED-22, pp. 945–946, Oct. 1975.

[3] D. Jäger, "Slow-wave propagation along variable Schottky-contact microstrip line," *IEEE Trans. Microwave Theory Tech.*, vol. MTT-24, pp. 566–573, Sept. 1976.

[4] H. Hasegawa and H. Okizaki, "M.I.S. and Schottky slow-wave coplanar striplines on GaAs substrates," *Electron. Lett.*, vol. 13, pp. 663–664, 1977.

[5] H. Ogawa and T. Itoh, "Slow-wave characteristics of ferromagnetic semiconductor microstrip line," *IEEE Trans. Microwave Theory Tech.*, vol. MTT-34, pp. 1478–1482, Dec. 1986.

[6] K. Wu and R. Vahldieck, "Hybrid-mode analysis of homogeneously and inhomogeneously doped low-loss slow-wave coplanar transmission lines," *IEEE Trans. Microwave Theory Tech.*, vol. 39, pp. 1348–1360, Aug. 1991.

[7] R. Sorrentino, G. Leuzzi, and A. Silbermann, "Characteristics of metal–insulator–semiconductor coplanar waveguides for monolithic microwave circuits," *IEEE Trans. Microwave Theory Tech.*, vol. MTT-32, pp. 410–416, Apr. 1984.
[8] D. Jäger and J. P. Becker, "Distributed variable-capacitance microstrip lines for microwave applications," *Appl. Phys.*, vol. 12, pp. 203–207, 1977.
[9] K. Wu and R. Vahldieck, "Propagation characteristics of MIS transmission lines with inhomogeneous doping profile," *IEEE Trans. Microwave Theory Tech.*, vol. 38, pp. 1872–1878, Dec. 1990.
[10] Y. Fukuoka and T. Itoh, "Slow-wave coplanar waveguide on periodically doped semiconductor substrate," *IEEE Trans. Microwave Theory Tech.*, vol. MTT-31, pp. 1013–1017, Dec. 1983.
[11] S. Seki and H. Hasegawa, "Cross-tie slow-wave coplanar waveguide on semi-insulating GaAs substrates," *Electron. Lett.*, vol. 17, pp. 940–941, 1981.
[12] T. H. Wang and T. Itoh, "Compact grating structure for application to filters and resonators in monolithic microwave integrated circuits," *IEEE Trans. Microwave Theory Tech.*, vol. MTT-35, pp. 1176–1182, Dec. 1987.
[13] H. Kamitsuna and H. Ogawa, "Novel slow-wave meander lines using multilayer MMIC technologies," *IEEE Microwave Guided Wave Lett.*, vol. 2, pp. 8–10, Jan. 1992.
[14] F. R. Yang, Y. Qian, R. Coccioli, and T. Itoh, "A novel low-loss slow-wave microstrip structure," *IEEE Microwave Guided Wave Lett.*, vol. 8, pp. 372–374, Nov. 1998.
[15] Y. Qian, V. Radisic, and T. Itoh, "Simulation and experiment of photonic band-gap structures for microstrip circuits," in *Asia–Pacific Microwave Conf.*, Hong Kong, Dec. 1997, pp. 585–588.
[16] V. Radisic, Y. Qian, R. Coccioli, and T. Itoh, "Novel 2-D photonic bandgap structure for microstrip lines," *IEEE Microwave Guided Wave Lett.*, vol. 8, pp. 69–71, Feb. 1998.
[17] Q. Xue, K. M. Shum, and C. H. Chan, "Novel 1-D microstrip PBG cells," *IEEE Microwave Guided Wave Lett.*, vol. 10, pp. 403–405, Oct. 2000.
[18] H. Y. D. Yang, N. G. Alexopoulos, and E. Yablonovitch, "Photonic band-gap materials for high-gain printed circuit antennas," *IEEE Trans. Antenna Propagat.*, vol. 45, pp. 185–187, Jan. 1997.
[19] F. R. Yang, K. P. Ma, Y. Qian, and T. Itoh, "A uniplanar compact photonic-bandgap (UC-PBG) structure and its applications for microwave circuits," *IEEE Trans. Microwave Theory Tech.*, vol. 47, pp. 1509–1514, Aug. 1999.
[20] D. Sievenpiper, L. Zhang, R. F. J. Broas, N. G. Alexópolous, and E. Yablonovitch, "High-impedance electromagnetic surfaces with a forbidden frequency band," *IEEE Trans. Microwave Theory Tech.*, vol. 47, pp. 2059–2074, Nov. 1999.
[21] F. R. Yang, K. P. Ma, Y. Qian, and T. Itoh, "A novel TEM waveguide using uniplanar compact photonic-bandgap (UC-PBG) structure," *IEEE Trans. Microwave Theory Tech.*, vol. 47, pp. 2092–2098, Nov. 1999.
[22] C. K. Tzuang and Y. C. Chen, "Dispersion characteristics of microstrip with periodic perturbations," in *IEEE MTT-S Int. Microwave Symp. Dig.*, June 2000, pp. 1537–1540.
[23] A. A. Oliner, "Radiating periodic structures: Analysis in terms of k vs. β diagrams," *Short Course Microwave Field Network Tech.*, June 4, 1963.
[24] Y. Hua and T. K. Sarkar, "Generalized pencil-of-function method for extracting poles of an EM system from its transient response," *IEEE Trans. Antennas Propagat.*, vol. 37, pp. 229–234, Feb. 1989.
[25] W. R. Eisenstadt and Y. Eo, "S-parameter-based IC interconnect transmission line characterization," *IEEE Trans. Comp., Hybrids, Manufact. Technol.*, vol. 15, pp. 483–490, Aug. 1992.
[26] F. R. Yang, R. Coccioli, Y. Qian, and T. Itoh, "Analysis and application of coupled microstrips on periodically patterned ground plane," in *IEEE MTT-S Int. Microwave Symp. Dig.*, Jun. 2000, pp. 1529–1532.
[27] G. L. Matthaei, L. Young, and E. M. T. Jones, *Microwave Filters, Impedance-Matching Networks, and Coupling Structures*. Norwood, MA: Artech House, 1980.

Ching-Kuo Wu (S'99) was born in Changhua, Taiwan, R.O.C., in 1971. He received the B.S. degree in electrical engineering from the National Cheng Kung University, Tainan, Taiwan, R.O.C., in 1993, the M.S. degree in communication engineering from the National Chiao Tung University, Hsinchu, Taiwan, R.O.C., in 1995, and is currently working toward the Ph.D. degree in communication engineering at National Chiao Tung University.

From 1997 to 1998, he was with the Computer and Communication Laboratories, Industrial Technology Research Institute, Hsinchu, Taiwan, R.O.C., where he was involved with the development of RF modules for a GSM/DCS1800 handset. His current research interests include the analysis and design of microwave and millimeter-wave components and PBG structures.

Hsien-Shun Wu (S'97–M'98) received the B.S. degree in electronic engineering from the National Taipei University of Technology, Taipei, Taiwan, R.O.C., in 1999, the M.S. degree in communication engineering from the National Chiao Tung University, Hsinchu, Taiwan, R.O.C. in 2001, and is currently working toward the Ph.D. degree in communication engineering from the National Chiao Tung University.

His research interests include RF module design and applications of PBG structures.

Ching-Kuang Cliver Tzuang (S'80–M'80–SM'92–F'99) received the B.S. degree in electronic engineering from the National Chiao Tung University, Hsinchu, Taiwan, R.O.C., in 1977, the M.S. degree from the University of California at Los Angeles, in 1980, and the Ph.D. degree in electrical engineering from the University of Texas at Austin, in 1986.

From 1981 to 1984, he was with TRW, Redondo Beach, CA, where he was involved with analog and digital MMICs. Since 1986, he has been with the Institute of Communication Engineering, National Chiao Tung University. His research activities involve the design and development of millimeter-wave and microwave active and passive circuits and the field theory analysis and design of various complex waveguiding structures and large-array antennas. He has supervised 58 M.S. students and 15 Ph.D. students.

Dr. Tzuang helped in the formation of the IEEE Microwave Theory and Techniques Society (IEEE MTT-S) Taipei chapter, and served as secretary, vice chairman, and chairman in 1988, 1989, and 1990, respectively. He has been on the Asia–Pacific Microwave Conference International Steering Committee, where, since 1994, he has represented the Taipei chapter as the international liaison officer.